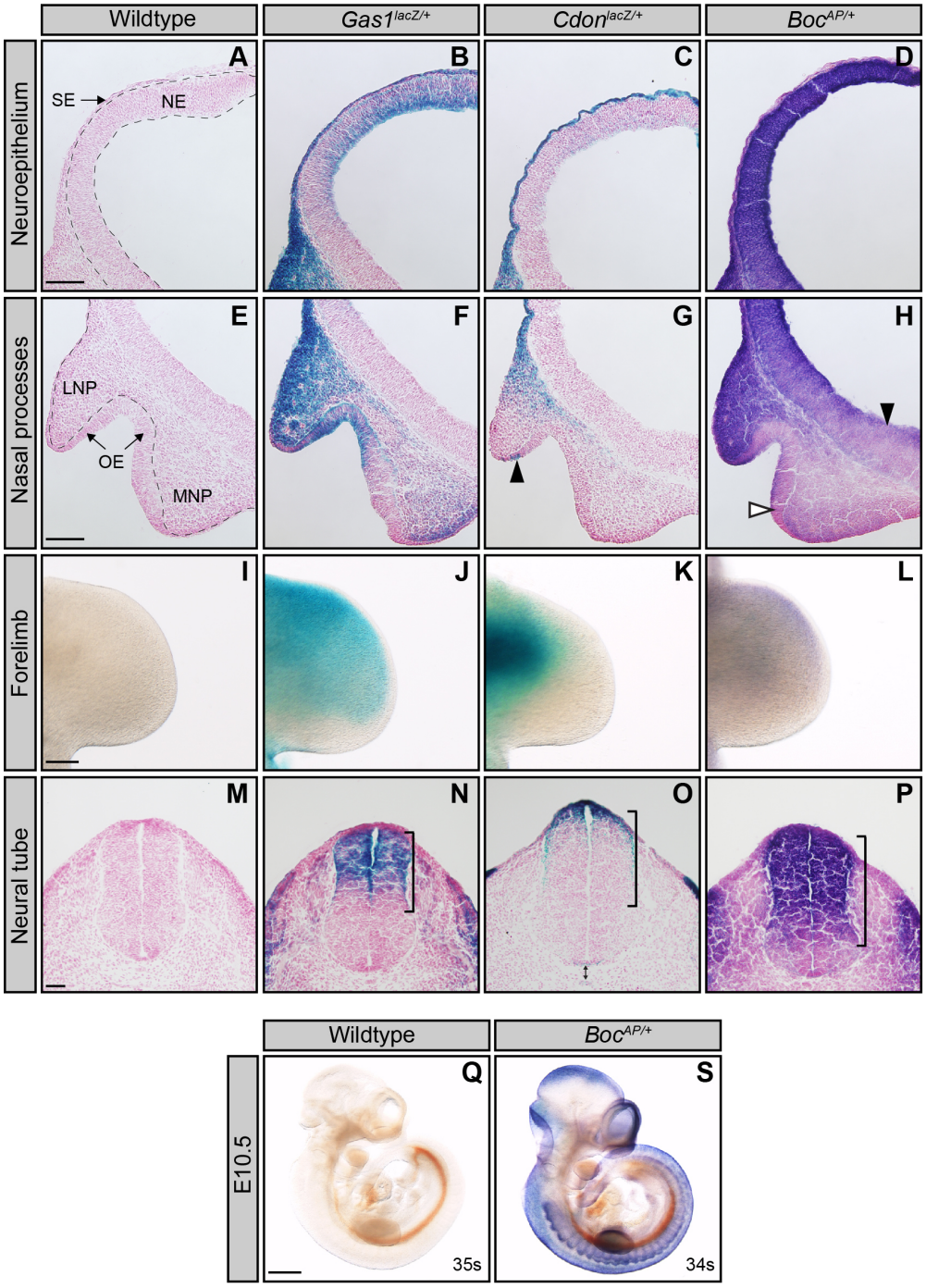

Figure S1. *Gas1, Cdon* and *Boc* are differentially expressed across multiple HH-responsive tissues.

Analysis of HH co-receptor expression using *lacZ* (*Gas1*, *Cdon*) and *hPLAP* (*Boc*) reporter alleles in HH-responsive tissues (A-P). High magnification pictures of coronal sections of E10.5 forebrains (A-H; cf. Fig.1Q-T), from wildtype (A, E), $Gas1^{lacZ/+}$ (B, F), $Cdon^{lacZ/+}$ (C, G), and $Boc^{AP/+}$ (D, H) embryos are shown. E10.5 forebrain neuroepithelia (A-D) and nasal processes (E-H). Arrowhead in (G) denotes a subset of cells expressing *Cdon* in the olfactory epithelium. Black arrowhead in (H) identifies the extended ventral expression of *Boc* closer to the telencephalon source of *Shh* expression. White arrowhead in (H) denotes *Boc* expression in the

olfactory epithelium. Whole mount X-Gal and Alkaline Phosphatase staining of E10.5 forelimb buds (I-L) from wildtype (I), *Gas1*$^{lacZ/+}$ (J), *Cdon*$^{lacZ/+}$ (K), and *Boc*$^{AP/+}$ (L) embryos. Transverse sections of E10.5 neural tubes (M-P) from wildtype (M), *Gas1*$^{lacZ/+}$ (N), *Cdon*$^{lacZ/+}$ (O), and *Boc*$^{AP/+}$ (P) embryos. Black brackets denote the expression domain of the HH co-receptors in the neural tube. Double-headed arrow in (O) indicates *Cdon* expression in the floor plate and notochord. Heat inactivation of endogenous alkaline phosphatase at E10.5 in wildtype (Q) and *Boc*$^{AP/+}$ (S) animals demonstrates the specificity of alkaline phosphatase staining. Somite number (s) is indicated in the lower right corner (Q-S). Scale bars, (A-H) 100µm, (I-L) 200µm, (M-P) 50µm, (Q-S) 500µm. Abbreviations: surface ectoderm (SE), neuroepithelium (NE), lateral nasal process (LNP), medial nasal process (MNP), olfactory epithelium (OE).

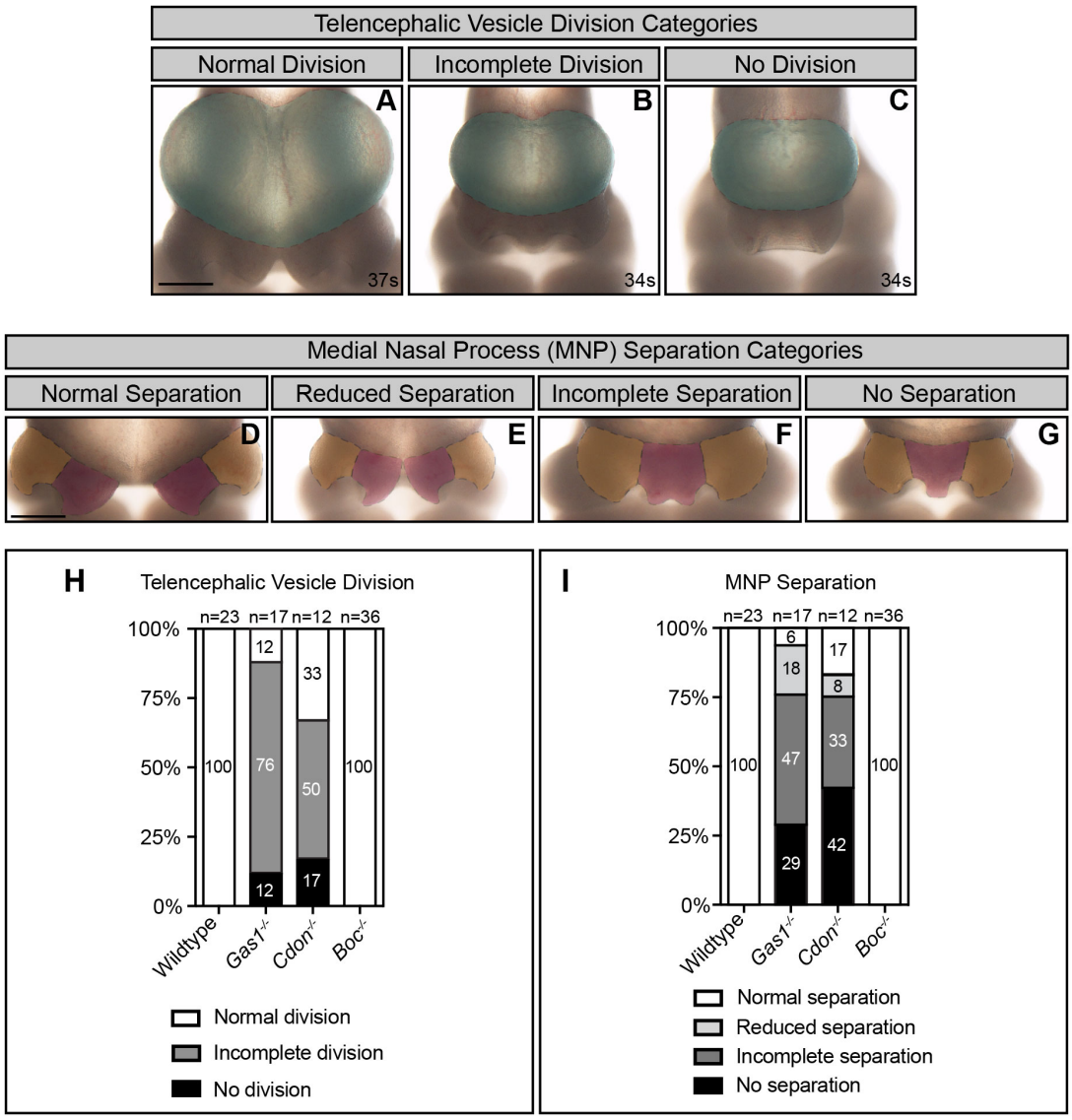

Figure S2. Telencephalic vesicle division and MNP separation in *Gas1*, *Cdon* and *Boc* mutants.

En face view of E10.5 embryos (A-C). The telencephalic vesicles are pseudocolored in green and surrounded by a dotted line. Telencephalic vesicle division classification categories: normal division (A), incomplete division (B), no division (C). Midface view of E10.5 embryos (D-G). The lateral and medial nasal processes are pseudocolored in orange and red, respectively, and are surrounded by a dotted line. Medial nasal process (MNP) classification categories: normal separation (D), reduced separation (E), incomplete separation (F), and no separation (G). Scale bars (A, D), 500µm. Telencephalic vesicle (TV) division frequency in E10.5 wildtype (n=23), *Gas1*$^{-/-}$ (n=17), *Cdon*$^{-/-}$ (n=12), and *Boc*$^{-/-}$ (n=36) embryos (H). Medial nasal process (MNP) separation frequency in E10.5 wildtype (n=23), *Gas1*$^{-/-}$ (n=17), *Cdon*$^{-/-}$ (n=12), and *Boc*$^{-/-}$ (n=36) embryos (I).

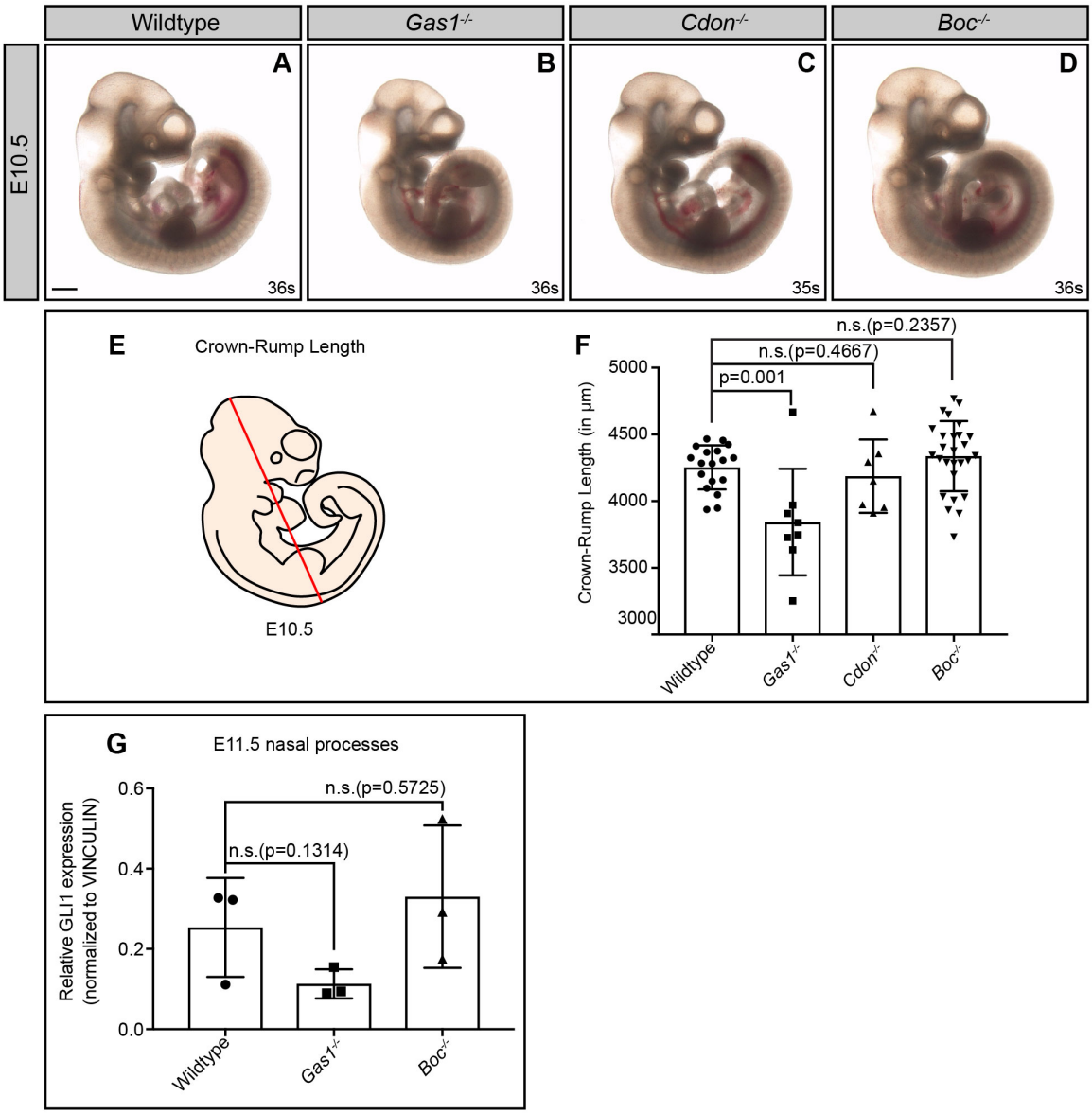

Figure S3. Reduced embryo size in E10.5 *Gas1*, but not *Cdon* or *Boc*, mutant embryos. Sagittal views of E10.5 wildtype (A), *Gas1*$^{-/-}$ (B), *Cdon*$^{-/-}$(C), and *Boc*$^{-/-}$(D) embryos. Scale bar (A), 500 µm. Schematic sagittal view of an E10.5 mouse embryo (E); the red diagonal line denotes crown-rump length. Crown-rump length quantitation of E10.5 wildtype (n= 18), *Gas1*$^{-/-}$ (n=8), *Cdon*$^{-/-}$ (n=7), *Boc*$^{-/-}$ (n=27) embryos (F). Quantitation of GLI1 levels in nasal processes isolated from E11.5 wildtype (n=3), *Gas1*$^{-/-}$ (n=3) and *Boc*$^{-/-}$ (n=3) embryos (G). Data are mean ±s.d. P-values were determined by a two-tailed Student's *t*-test. The Bonferroni correction was employed to account for multiple comparisons in each dataset; (F) non-significant (n.s.; $p>0.0166$), significant ($p\leq0.0166$) and (G) non-significant (n.s.; $p>0.0250$), significant ($p\leq0.0250$).

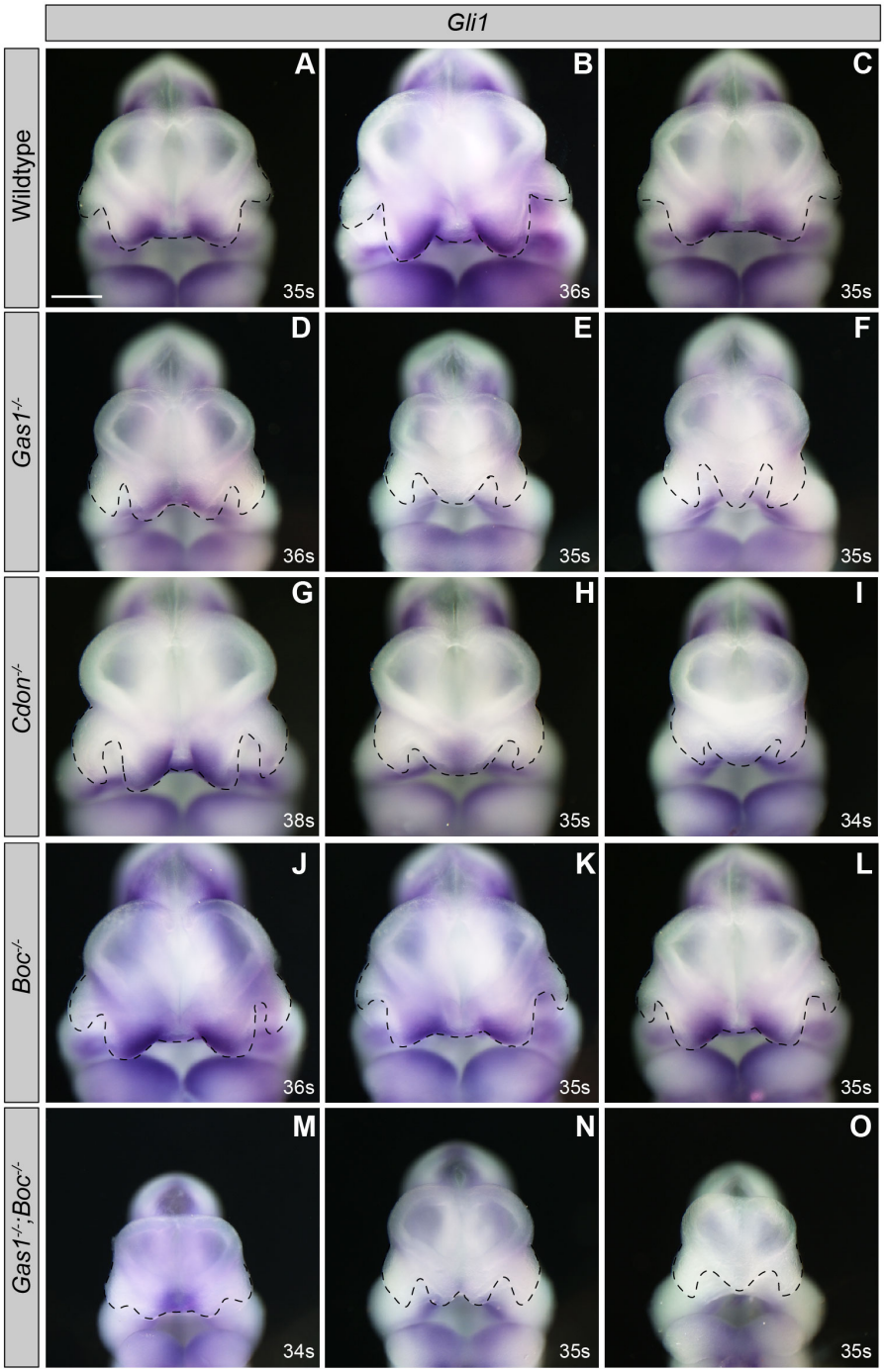

Figure S4. The spectrum of HPE phenotypes correlates with changes in *Gli1* expression. *In situ* hybridization detection of *Gli1* expression in E10.5 forebrains (A-O). *En face* views of E10.5 forebrains from wildtype (A-C), *Gas1*$^{-/-}$ (D-F), *Cdon*$^{-/-}$ (G-I), *Boc*$^{-/-}$ (J-L) and *Gas1*$^{-/-}$*;Boc*$^{-/-}$ (M-O) embryos are shown. Somite number (s) is indicated in the lower right corner of each panel. Black dotted lines outline nasal processes. Notice that as the HPE phenotypes worsen (from left to right) in *Gas1* and *Cdon* mutants, the expression of *Gli1* in the MNP is lost. *Boc* mutants display equal levels of *Gli1* in the MNP and do not display any gross craniofacial defects. *Gas1;Boc* double mutants with ameliorated craniofacial defects (from left to right) maintain *Gli1* expression in the MNP, while *Gli1* expression is lost in mutants that display severe craniofacial defects. Scale bars (A-O), 500 μm.

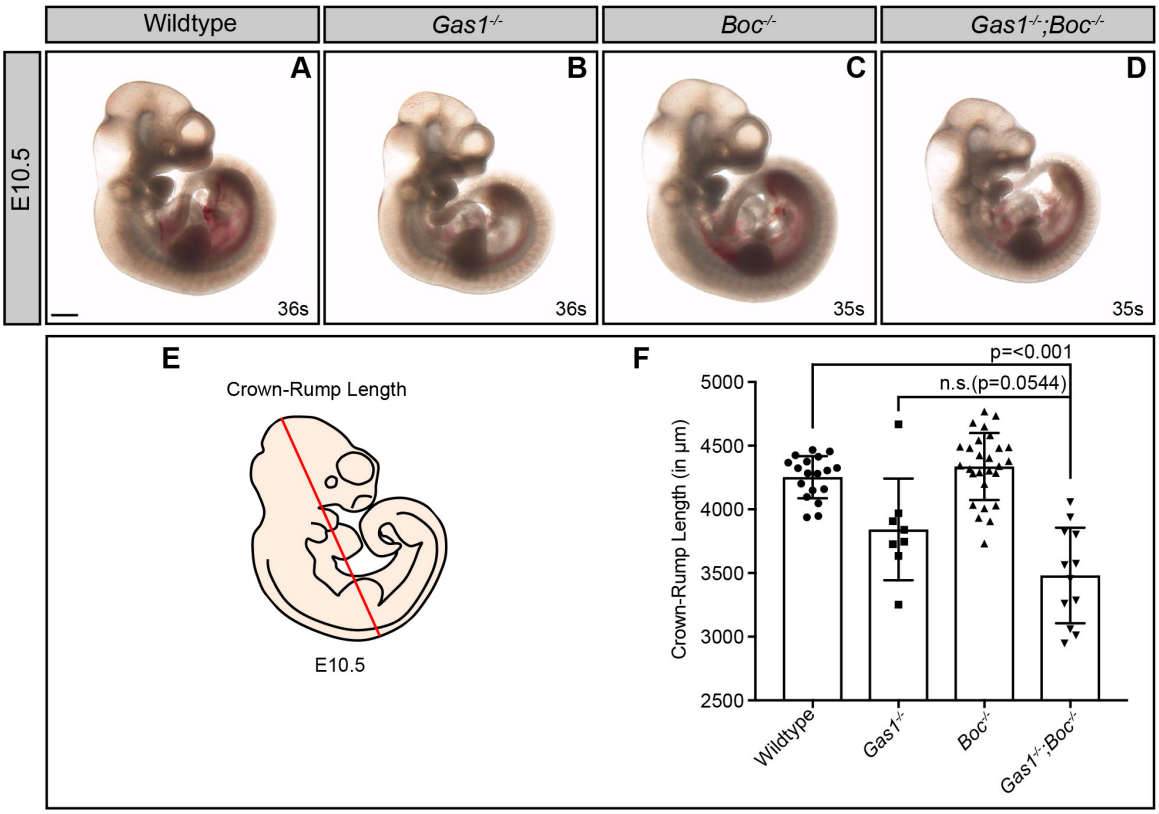

Figure S5. Reduced Crown-Rump Length in E10.5 *Gas1;Boc* double mutant embryos. Sagittal view of E10.5 wildtype (A), *Gas1*$^{-/-}$ (B), *Boc*$^{-/-}$ (C), and *Gas1*$^{-/-}$*;Boc*$^{-/-}$ (D) embryos. Schematic sagittal view of an E10.5 mouse embryo; the red diagonal line denotes the crown-rump length (E). Crown-rump length quantitation in wildtype (n= 18), *Gas1*$^{-/-}$ (n=8), *Boc*$^{-/-}$ (n=27), and *Gas1*$^{-/-}$*;Boc*$^{-/-}$ (n=12) embryos (F). Scale bar in A, 500µm. Data are mean±s.d. P-values were determined by a two-tailed Student's *t*-test. The Bonferroni correction was employed to account for multiple comparisons in each dataset; (F) non-significant (n.s.; p>0.0250), significant (p≤0.0250).

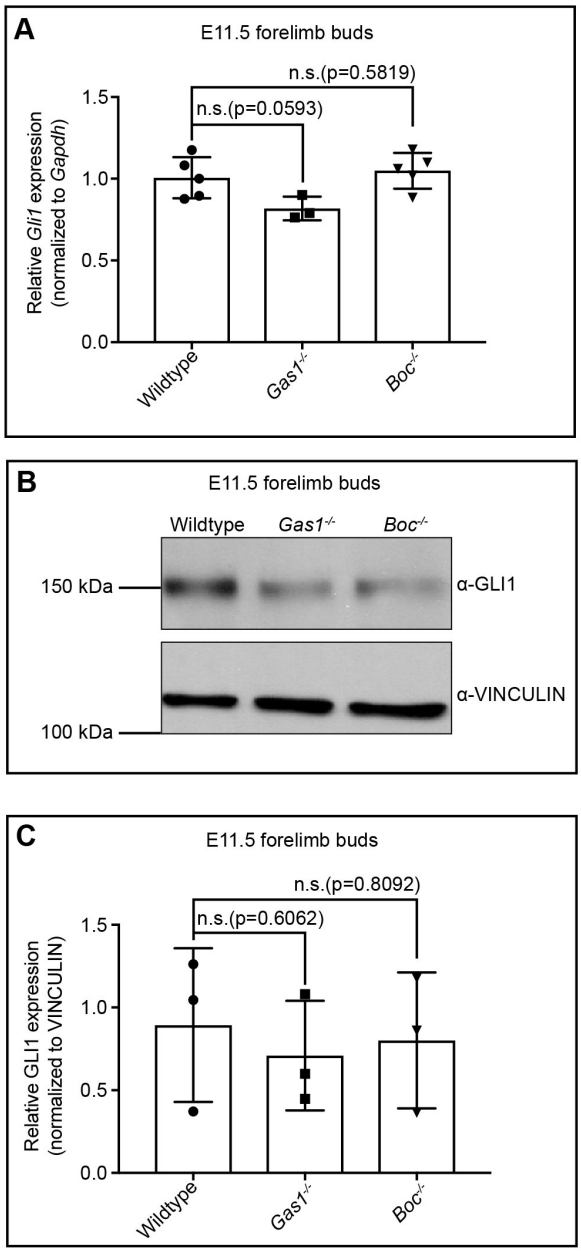

Figure S6. *Gli1* mRNA and protein levels in E10.5 *Gas1* and *Boc* mutant forelimb buds. Relative expression of *Gli1* by qRT-PCR in forelimb buds (A) of E11.5 wildtype (n=5), *Gas1*$^{-/-}$ (n=3) and *Boc*$^{-/-}$ (n=5) embryos normalized to *Gapdh.* Biological replicates were analyzed in triplicate. Western blot analysis of GLI1 endogenous protein in forelimb buds (B). Anti-VINCULIN was used as loading control, three biological replicates were analyzed. Quantitation of GLI1 levels in forelimb buds (C) of E11.5 wildtype (n=3), *Gas1*$^{-/-}$ (n=3) and *Boc*$^{-/-}$ (n=3) embryos. Data are mean±s.d. P-values were determined by a two-tailed Student's *t*-test. The Bonferroni correction was employed to account for multiple comparisons in each dataset; (A,C) non-significant (n.s.; p>0.0250), significant (p≤0.0250).

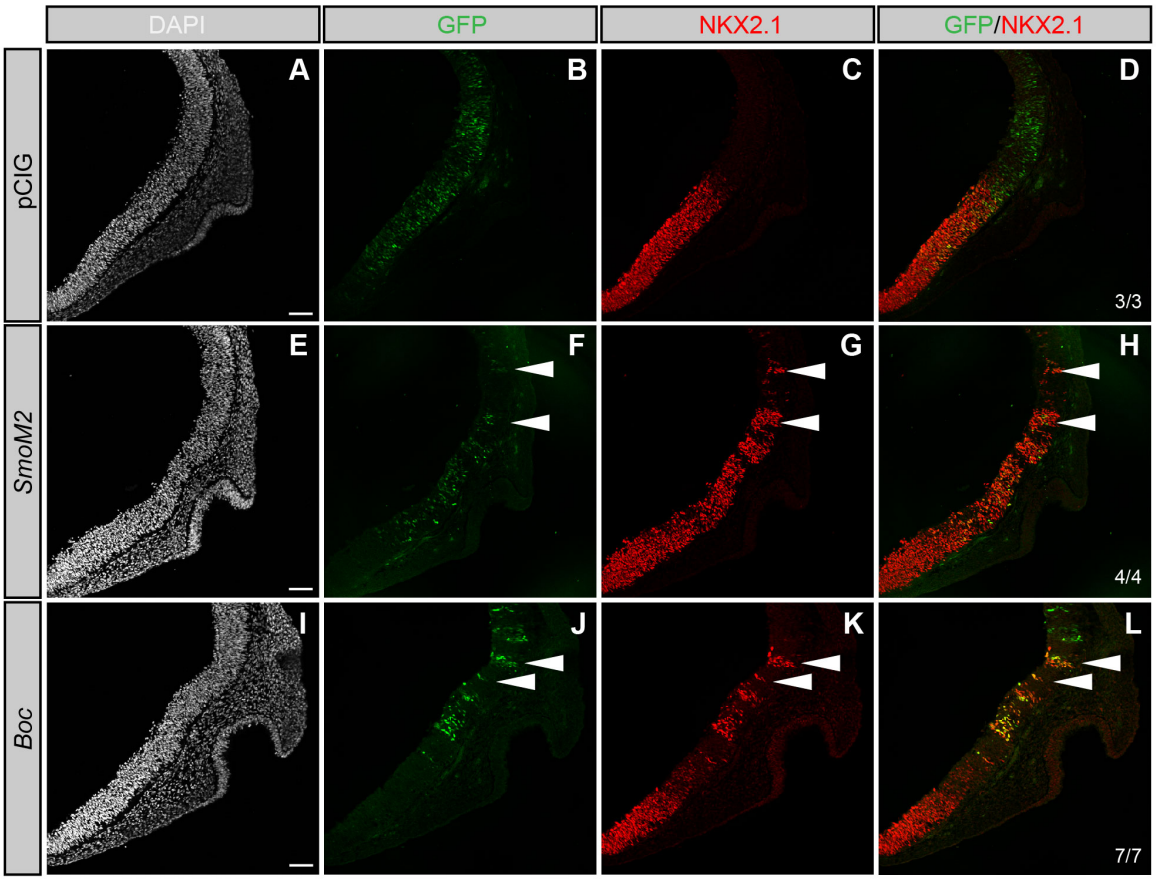

Figure S7. Boc promotes HH-dependent neural patterning in the developing chicken forebrain. Coronal sections of Hamburger-Hamilton stage 21-22 chicken forebrains electroporated with empty vector (pCIG; A-D), *SmoM2* (E-H), and *Boc* (I-L). DAPI (grayscale; A,E,I) denotes nuclei. GFP+ cells (green; B,F,J) identify electroporated cells. Antibody detection of NKX2.1 (red; C,G,K) reads out HH pathway activity. Merged images are shown in (D,H,L). The number of electroporated embryos that display ectopic NKX2.1 expression is indicated in the lower right corner (D,H,L). White arrowheads highlight ectopic NKX2.1 expression. Scale bars in A, E, and I, 50µm.

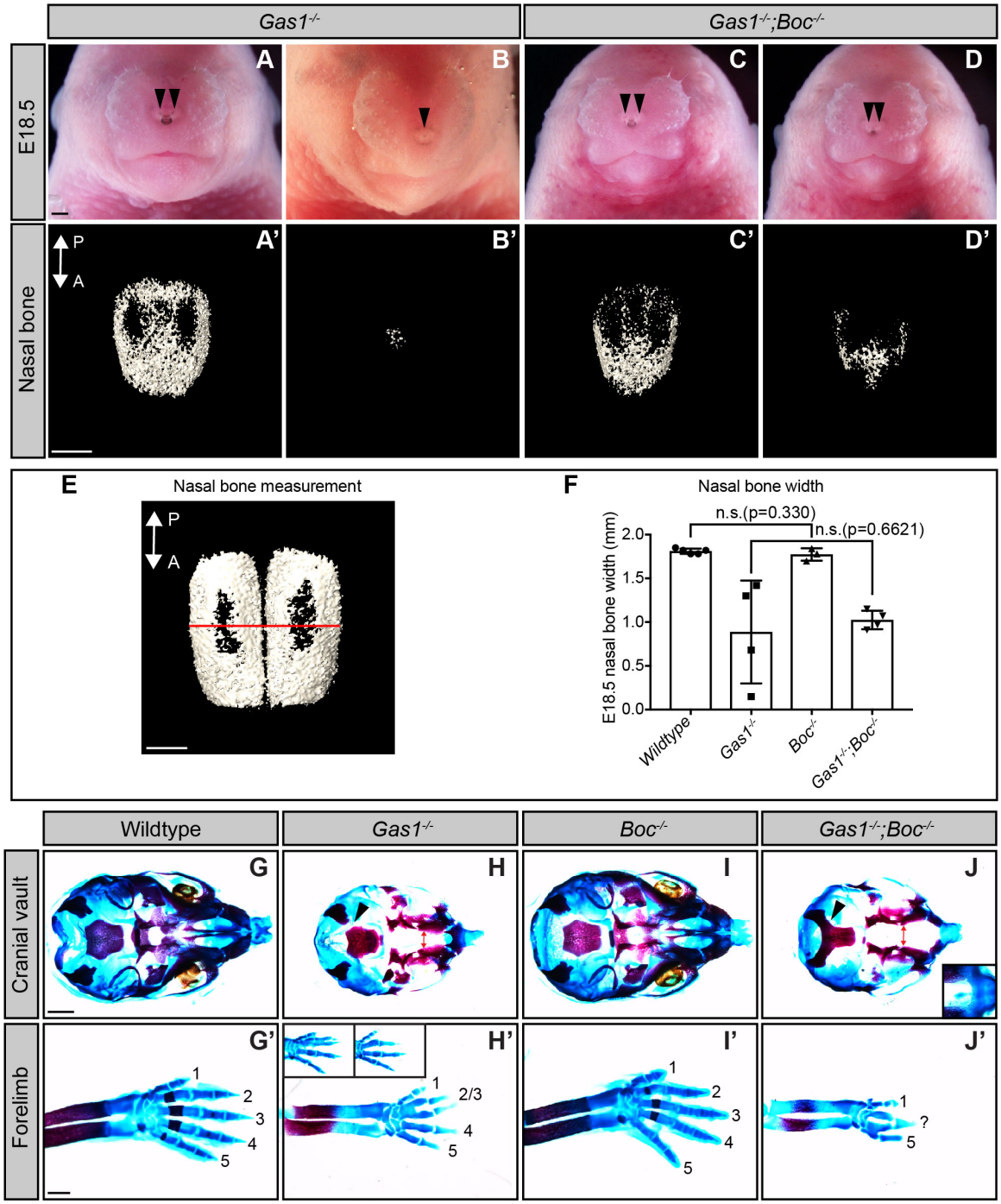

Figure S8. HPE phenotypes and digit specification defects in E18.5 *Gas1;Boc* mutant embryos.

En face view of E18.5 *Gas1*$^{-/-}$ (A,B) and *Gas1*$^{-/-}$*;Boc*$^{-/-}$ (C,D) embryos. Black arrowheads denote the nasal pits. Three dimensional reconstructions of microCT images of isolated nasal bones from E18.5 *Gas1*$^{-/-}$ (A',B') and *Gas1*$^{-/-}$*;Boc*$^{-/-}$ (C',D') embryos. A←→P specifies the anterior to posterior axis in (A'-D',E). MicroCT image of an isolated nasal bone from E18.5 wildtype embryo (E); the red horizontal line denotes the nasal bone width. Nasal bone width quantitation in wildtype (n=5), *Gas1*$^{-/-}$ (n=4), *Boc*$^{-/-}$ (n=3), and *Gas1*$^{-/-}$*;Boc*$^{-/-}$ (n=4) embryos (F). Data are

mean±s.d. P-values were determined by a two-tailed Student's *t*-test. The Bonferroni correction was employed to account for multiple comparisons in each dataset; (F) non-significant (n.s.; $p>0.0250$), significant ($p\leq0.0250$). Ventral views of E18.5 cranial vaults from wildtype (G), *Gas1*$^{-/-}$ (H), *Boc*$^{-/-}$ (I), and *Gas1*$^{-/-}$*;Boc*$^{-/-}$ (J) embryos, stained with Alcian Blue and Alizarin Red. Red double arrows denote the cleft palate in *Gas1*$^{-/-}$ and *Gas1*$^{-/-}$*;Boc*$^{-/-}$ embryos and black arrowheads mark occipital bone. Inset in (J) indicates hypoplastic premaxilla in *Gas1*$^{-/-}$*;Boc*$^{-/-}$ embryos. Forelimbs of E18.5 wildtype (G'), *Gas1*$^{-/-}$ (H'), *Boc*$^{-/-}$ (I'), and *Gas1*$^{-/-}$*;Boc*$^{-/-}$ (J') embryos, stained with Alcian Blue and Alizarin Red. Numbers denote specific digits where 1 is the most anterior and 5 is the most posterior. Insets in (H') demonstrate variable digit specification phenotypes in *Gas1*$^{-/-}$ embryos, which display either partial fusion of digits two and three (left), or the absence of either digit two or three (right). *Gas1*$^{-/-}$*;Boc*$^{-/-}$ embryos exhibit a more severe limb phenotype where only digits 1 and 5 can be clearly identified; a third, unidentified digit is labeled with a question mark (Allen et al., 2011). Scale bars (A,A',E,G',G'), 500 μm.

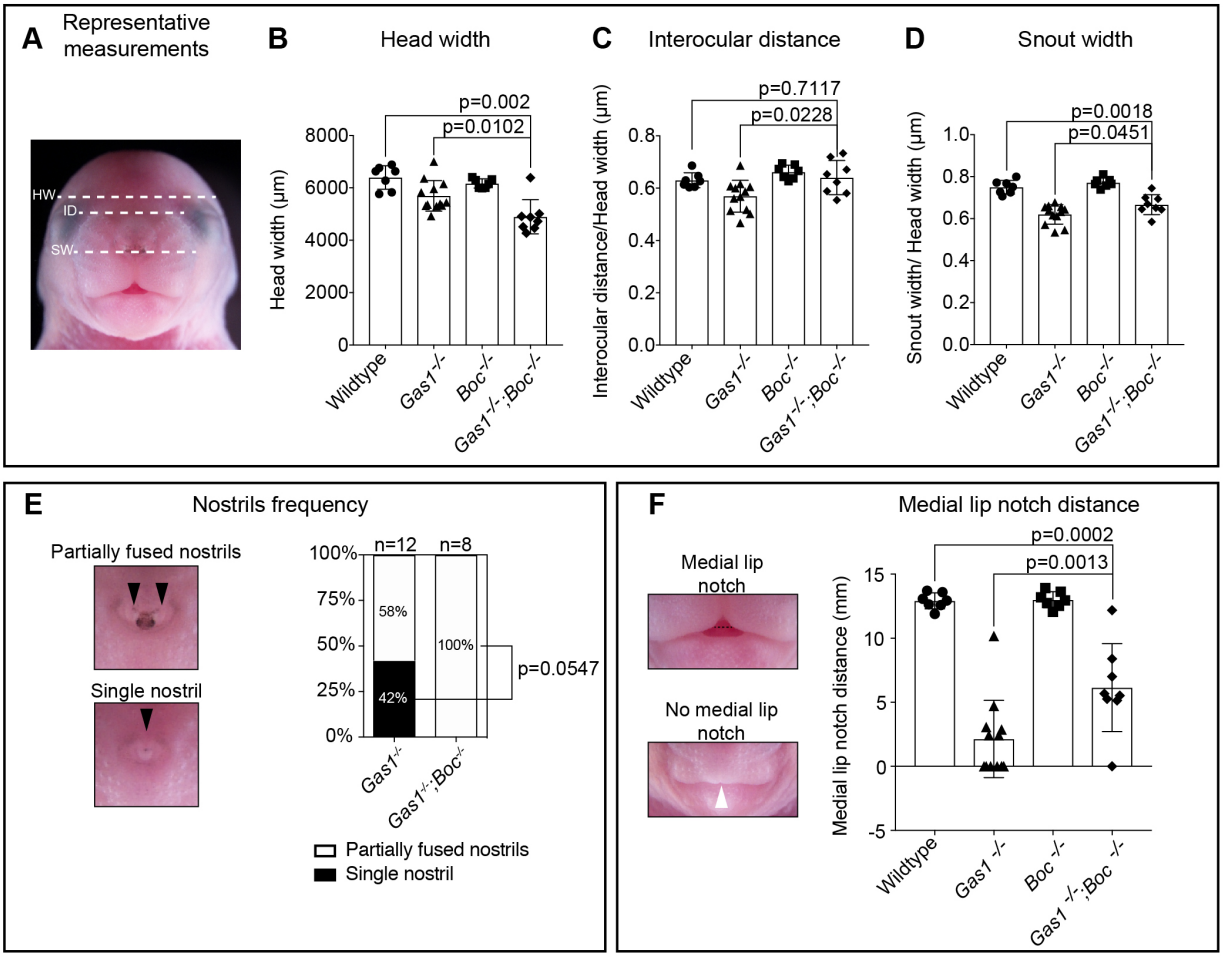

Figure S9. E18.5 *Gas1;Boc* mutants display partially ameliorated midfacial defects. Quantitation of anatomical landmarks in E18.5 embryos (A-F). Representative measurements of head width (HW), interocular distance (ID), snout width (SW) in E18.5 embryos (A). White dotted lines denote the measured distance. Head width quantitation in wildtype (n=7), *Gas1*$^{-/-}$ (n=12), *Boc*$^{-/-}$ (n=7) and *Gas1*$^{-/-}$*;Boc*$^{-/-}$ (n=8) embryos (B). Interocular distance quantitation, normalized to the head width in wildtype (n=7), *Gas1*$^{-/-}$ (n=12), *Boc*$^{-/-}$ (n=7) and *Gas1*$^{-/-}$*;Boc*$^{-/-}$ (n=8) embryos (C). Snout width quantitation, normalized to the head width in wildtype (n=7), *Gas1*$^{-/-}$ (n=12) and *Gas1*$^{-/-}$*;Boc*$^{-/-}$ (n=8) embryos (D). Nostril frequency in *Gas1*$^{-/-}$ (n=12) and *Gas1*$^{-/-}$*;Boc*$^{-/-}$ (n=8) embryos (E). Left panel, representative images of two partially fused nostrils and a single nostril. Black arrowheads denote two nostrils and a single nostril. Right panel, observed nostril frequency. Medial lip notch distance quantitation in wildtype (n=7), *Gas1*$^{-/-}$ (n=12), *Boc*$^{-/-}$ (n=7) and *Gas1*$^{-/-}$*;Boc*$^{-/-}$ (n=8) embryos (F). Left panel, representative images of medial lip notch and no medial lip notch. Right panel, medial lip notch quantitation. White arrowhead denotes the lack of a medial lip notch. Data are mean±s.d. P-values were determined by a two-tailed Student's *t*-test (B-D, F) or a Fisher's Exact test (E). The Bonferroni correction was employed to account for multiple comparisons in (B-D, F); (n.s.; p>0.0250), significant (p≤0.0250).

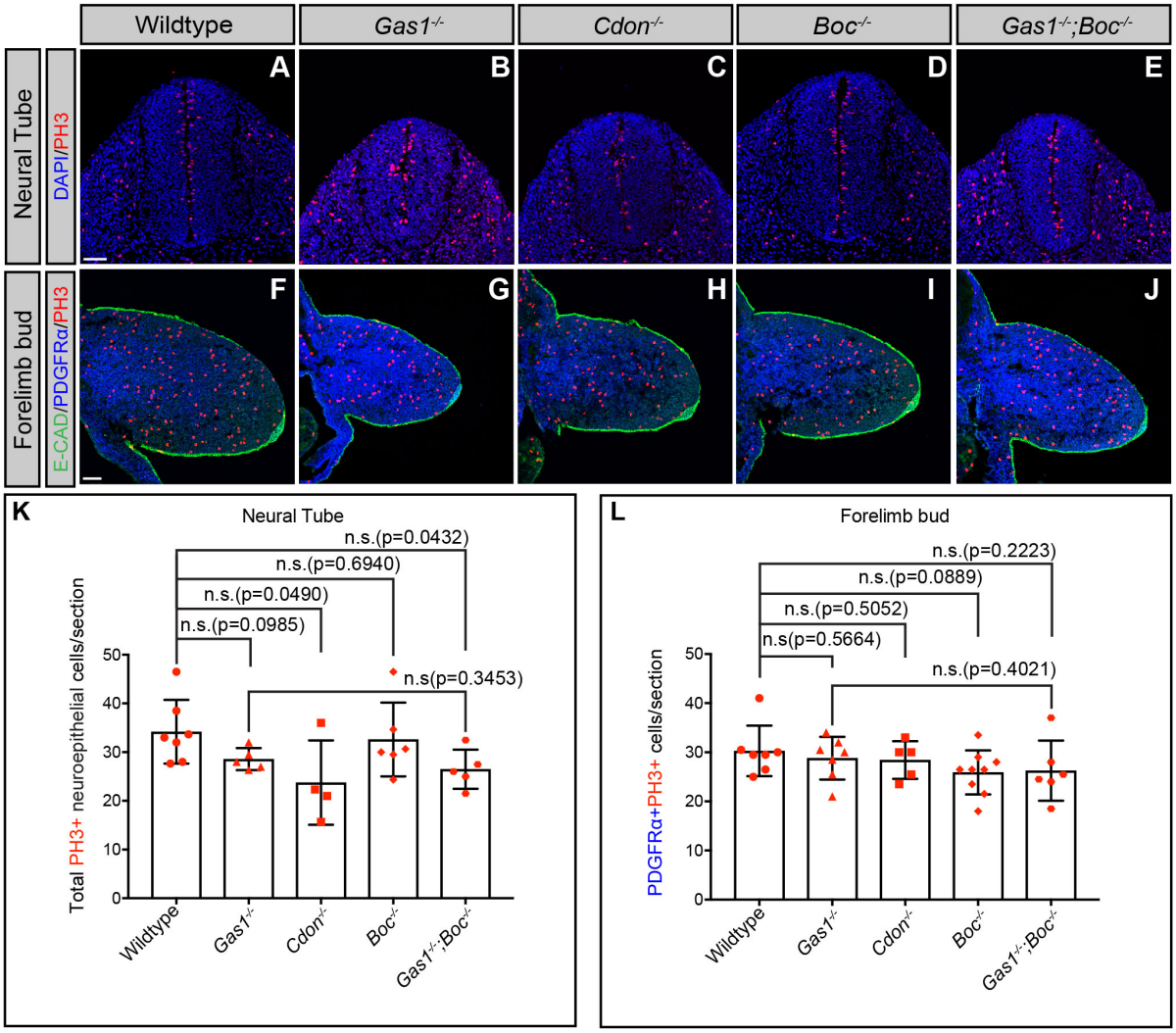

Figure S10. *Boc* does not contribute to neural tube or forelimb mesenchyme proliferation. Immunofluorescent analysis of proliferation in E10.5 neural tube (A-E) and forelimb (F-J) transverse sections from E10.5, wildtype (A,F), *Gas1*$^{-/-}$ (B,G), *Cdon*$^{-/-}$ (C,H), *Boc*$^{-/-}$ (D,I), and *Gas1*$^{-/-}$;*Boc*$^{-/-}$ (E,J) embryos. Antibody detection of E-CADHERIN (E-CAD, green, F-J), PDGFRα (blue, F-J), and phospho-histone H3 (PH3, red, A-J). Nuclei are stained with DAPI (blue, A-E). Quantitation of PH3+ cells (2 sections/embryo) in the neural tube (K) from E10.5 wildtype (n=7), *Gas1*$^{-/-}$ (n=5), *Cdon*$^{-/-}$ (n=4), *Boc*$^{-/-}$ (n=6) and *Gas1*$^{-/-}$;*Boc*$^{-/-}$ (n=5) embryos. Quantitation of PH3+ cells (2 sections/limb) in forelimb buds (L) from E10.5 wildtype (n=7), *Gas1*$^{-/-}$ (n=7), *Cdon*$^{-/-}$ (n=5), *Boc*$^{-/-}$ (n=9) and *Gas1*$^{-/-}$;*Boc*$^{-/-}$ (n=6) embryos. Data are mean±s.d. P-values were determined by a two-tailed Student's *t*-test. The Bonferroni correction was employed to account for multiple comparisons in each dataset; (K-L) non-significant (n.s.; p>0.0125), significant (p≤0.0125). Scale bars (A,F), 50 µm.

Table S1. General Reagents

Reagent	Vendor	Catalog number
Alcian Blue	Millipore Sigma	A5268
Alizarin Red	Millipore Sigma	A5533
Amersham ECL Prime Western Blotting Detection Reagent	GE Healthcare	RPN2232
Anti-Digoxigenin-Ap, Fab fragments	Roche	11 093 274 910
BM purple	Roche	11442074001
BSA	Millipore Sigma	A7906
Complete mini Protease Inhibitor Cocktail	Roche	1836153
DAPI	Thermo Fisher Scientific	D1306
EGTA	Millipore Sigma	E3889
EDTA	Thermo Fisher Scientific	S311-500
Fast green	Millipore Sigma	EM-4510
Formaldehyde	VWR	EMD-FX0410-5
Formamide	Millipore Sigma	4650-500ML
Glacial Acetic Acid	Thermo Fisher Scientific	BP2401-500
Glutaraldehyde	Millipore Sigma	G5882
Glycerol	VWR	EMGX0185-5
Goat serum	Thermo Fisher Scientific	16210064
High capacity cDNA reverse transcription kit	Applied Biosystems	4368814
Hyblot CL Autoradiography Film	Denville	E3018
Igepal (NP-40)	Millipore Sigma	I8896
Immu-mount	Thermo Fisher Scientific	9990412
Immuno-Blot PVDF membranes	Bio-Rad	162-0177
$K_3Fe(CN)_6$	Millipore Sigma	PX1455
$K_4Fe(CN)_6$	Millipore Sigma	P9387
$MgCl_2$	VWR	0288-500G
NaCl	Millipore Sigma	SX0420-3
Na deoxycholate	VWR	SX0480-2
OCT	Thermo Fisher Scientific	23730571
Paraformaldehyde	Thermo Fisher Scientific	50980489
Permount	Thermo Fisher Scientific	SP15100
Pierce BCA protein assay kit	Thermo Fisher Scientific	PI23225

Polyethyleneglycol	Millipore Sigma	91893-1L-F
Potassium hydroxide	VWR	PX1490-1
PowerUP SYBR Green Master Mix	Applied Biosystems	A25742
Proteinase K	Roche	03115836001
Quick-RNA micro prep	Zymo Research	R1055
Sheep serum	Bioworld	30611168-1
Tris	VWR	JT4109-2
Triton X-100	VWR	9410
Tween-20	VWR	9480
X-gal	Goldbio	X4281C
Xylenes	VWR	XX00555

Table S2. Primary and secondary antibodies used for immunofluorescence

Primary antibodies	Vendor	Catalog number	Dilution
NKX2.1 (rabbit IgG)	Abcam	ab76013	1:200
E-CADHERIN (mouseIgG2a)	BD Biosciences	610181	1:500
NKX2.2 (mouseIgG2b)	Developmental Studies Hybridoma Bank	74.5A5	1:20
OLIG2 (rabbit IgG)	Millipore Sigma	AB9610	1:2,000
NKX6.1 (mouseIgG1)	Developmental Studies Hybridoma Bank	F55A10	1:20
Phospho-histone H3 (rabbit IgG)	Millipore Sigma	06-570	1:1,000
Phospho-histone H3 (mouse IgG1)	Cell Signaling Technology	9706S	1:100
PDGFRα (rabbit IgG)	Cell Signaling Technology	3174S	1:100
Secondary antibodies	Vendor	Catalog number	Dilution
Alexa Fluor 488 (Goat anti-Rabbit IgG)	Thermo Fisher Scientific	A-11008	1:500
Alexa Fluor 555 (Goat anti-Mouse IgG2b)		A-21147	
Alexa Fluor 488 (Goat anti-Mouse IgG2a)		A-21131	
Alexa Fluor 555- (Goat anti-Rabbit IgG)		A-21428	
Alexa Fluor 488 (Goat anti-Mouse IgG1)		A-21121	
Alexa Fluor 555 (Goat anti-Mouse IgG2a)		A-21137	
Alexa Fluor 647 (Goat anti-Mouse IgG1)		A-21240	

Table S3. Western Blot antibodies

Primary antibodies	Vendor	Catalog number	Dilution
Gli1 (V812) (rabbit IgG)	Cell Signaling Technology	#2354	1:1,000
Vinculin (E1E9V) XP (rabbit IgG)	Cell Signaling Technology	#13901	1:1,000
Secondary antibodies	Vendor	Catalog number	Dilution
Peroxidase conjugated AffiniPure F(ab)2 Fragment Donkey Anti- Rabbit IgG	Jackson ImmunoResearch	711-036-152	1:10,000

Table S4. qRT-PCR Primers

Gene	Sequence	Source
Gli1-F	GTGCACGTTTGAAGGCTGTC	(Han et al., 2017)
Gli1-R	GAGTGGGTCCGATTCTGGTG	
Gapdh-F	GGTGAAGGTCGGTGTGAACG	(Lewandowski et al., 2015)
Gapdh-R	CTCGCTCCTGGAAGATGGTG	

Supplementary Information References

Allen, B. L., Song, J. Y., Izzi, L., Althaus, I. W., Kang, J. S., Charron, F., Krauss, R. S. and McMahon, A. P. (2011). Overlapping roles and collective requirement for the coreceptors GAS1, CDO, and BOC in SHH pathway function. *Dev Cell* **20**, 775-787.

Han, Y., Xiong, Y., Shi, X., Wu, J., Zhao, Y. and Jiang, J. (2017). Regulation of Gli ciliary localization and Hedgehog signaling by the PY-NLS/karyopherin-beta2 nuclear import system. *PLoS Biol* **15**, e2002063.

Lewandowski, J. P., Du, F., Zhang, S., Powell, M. B., Falkenstein, K. N., Ji, H. and Vokes, S. A. (2015). Spatiotemporal regulation of GLI target genes in the mammalian limb bud. *Dev Biol* **406**, 92-103.